Correlation between microstructure and mechanical behaviour at high temperatures of a SiC fibre with a low oxygen content (Hi–Nicalon)

G. CHOLLON, R. PAILLER, R. NASLAIN
Laboratoire des composites Thermostructuraux, 3, allée de La Boétie, 33600 Pessac, France
P. OLRY
Société Européenne de Propulsion, 33165 Saint Médard en Jalles, France

An oxygen free Si–C fibre has been studied in terms of the chemical, structural and mechanical properties produced as a function of annealing treatments. In spite of its high thermal stability with regard to a Si–C–O fibre the Si–C fibre was subject to moderate SiC grain growth, organization of the free carbon phase and densification within the temperature range 1200–1400 °C. The strength reduction at ambient for temperatures $\leqslant$ 1600 °C could possibly be due to SiC coarsening or superficial degradation. Bend stress relaxation (BSR) and tensile creep tests show that the as-received fibre undergoes a viscous flow from 1000 °C. The thermal dependance of the creep strain rate strongly increases at temperatures $\geqslant$ 1300 °C. This feature might be partly explained by the structural evolution of the fibre occurring above this temperature. Heat treated fibres (1400–1600 °C) exhibit a much better creep strength, probably due to their improved structural organization.

1. Introduction

Composite materials for application in severe conditions (high temperature, high loading and long duration), require fibrous reinforcements with excellent mechanical properties, chemical and structural stability and oxidation resistance at high temperatures [1–4].

Carbon fibres exhibit high stiffness (E), fracture strength (σ^R) and creep resistance at high temperatures under an inert atmosphere [5, 6], but they are highly sensitive to oxidation at a temperature as low as 450 °C [6, 7]. Oxide fibres such as alumina, zirconia and more recently Yttrium Aluminium Garnet (YAG) are thermally stable under an oxidizing atmosphere, but they have a poor creep resistance at high temperatures [8–10]. Silicon carbide is one of the best materials for the reinforcement of Ceramic mature composites (CMCs). In fact, SiC has excellent mechanical properties at high temperatures (σ^R, E, creep resistance) [1–3] coupled with a rather good oxidation resistance [1–4, 11, 12].

Yajima *et al.* were the first to prepare SiC-based fibres with a small diameter ($d \approx 14$ μm) (i.e., that were weavable). The preparation of the fibres involved the spinning of molten polycarbosilane (PCS), the curing of the green filaments in an oxidizing atmosphere and pyrolysis in an inert atmosphere [13, 14]. Such fibres are available under the trade name Nicalon. Unfortunately a lack of stability limits their use to temperatures below 1200 °C which is due to their chemical composition and structure. The fibre consists of β-SiC nanocrystals (of size $\sim$2 nm) as well as free carbon in the form of basic structural units (BSU: turbostratic stacks of 2–3 aromatic carbon layers of about 10 cycles) which are embedded within an intergranular amorphous material (SiC_xO_y) [15–17]. The silicon oxycarbide phase undergoes decomposition at about 1200 °C with an evolution of carbon and silicon monoxides, an oxidation of free carbon and a crystallisation of the β-SiC phase [18–21]. The decomposition of the fibre results in a significant reduction in the mechanical properties (σ^R, E) [22, 23]. On the other hand, the oxycarbide phase which is a compliant material, is also responsible for the low creep resistance of Si–C–O fibre [24, 25].

Okamura *et al.* have developed a physical curing process using electron beam irradiation under an inert atmosphere. The cross-linking of the polymeric framework is thus achieved according to the homolytic ruptures of the side chain functions and the combination of radicals into a three dimensional PCS structure, which is accompanied by an evolution of gaseous species (H_2, CH_4) [26]. The advantage of this process is that it does not introduce oxygen. As a consequence, the Si–C fibres are reported to be much more heat-resistant than the Si–C–O fibres [26–28]. The nanotexture of this experimental fibre is apparently simpler than that of the Si–C–O fibre being mostly composed of β-SiC nanocrystals and free carbon [29, 30].

The aim of the present work is to characterize the mechanical behaviour of such fibres at high temper-

0022–2461

atures, especially after heat treatments at increasing temperatures (T_p). Correlations between (i) the chemical and structural change as a function of T_p and (ii) the mechanical properties at high temperatures have also been established. In addition simple mechanisms are suggested to explain the mechanical behaviour of the fibres as a function of the testing temperature.

2. Experimental procedure

2.1. Annealing treatments

The annealing treatments were performed with a high-temperature rig consisting of a graphite crucible heated with a radio frequency coil that has been described elsewhere [30]. The samples were rapidly heated (30 °C min^{-1}) and maintained at the annealing temperature T_p ($1200 < T_p < 2000$ °C) under a high-purity argon atmosphere (100 kPa) during a time t_p ($1h < t_p < 10h$). The argon used was grade N56 from Alphagaz.

2.2. Physical, chemical and structural analyses

The elemental analysis of the fibres was performed using electron probe microanalysis (EPMA). The silicon, carbon and oxygen atomic percentage were determined in the wavelength dispersion (WDS) mode by mean of a thallium acid phthalate (TAP) crystal for Si–K_α and a pseudo-crystal PC2 multilayer crystal for C–K_α and O–K_α. Chemical standards assumed to be stoichiometric were used for calibration: SiC (for silicon and carbon) and SiO_2 (for oxygen). The chemical analysis of the as-received fibres was also investigated by usual elemental analysis techniques at the Service Central d'Analyse at CNRS, Vernaison, France.

The morphology of the creep tested fibres were studied by scanning electron microscopy (SEM) using a JEOL 8405 microscope. The structure of the monofilaments was studied at the nanometer scale by high resolution transmission electron microscopy (TEM) using a Philips EM400 microscope. The samples were prepared according to the following procedure: the fibres were embedded in an epoxy resin which was cut into thin foils with an ultramicrotom. The TEM analyses were performed in the bright field (BF), dark field (DF), lattice fringe (LF) and selected area diffraction (SAD) modes.

The X-ray diffraction (XRD) spectra were recorded on a SIEMENS D5000 diffractometer using (Cu–K_α) radiation and data were measured on a tow of fibres which had been successively heat-treated at increasing temperatures. The apparent mean grain size (L) of the β-SiC crystalline phase present in the samples was calculated from the width (D) of the (1 1 1) diffraction peak at mid-height, according to the following equation:

$$L = \frac{K\lambda}{D.\cos\theta} \quad (1)$$

where K is a constant (taken as 1), λ the Cu–K_α wavelength (i.e., $\lambda = 0.154$ nm) and θ the Bragg angle ($\theta = 17.8^\circ$ for β-SiC (1 1 1)).

The density of the samples was measured using helium-pycnometry on filament tows using an Accupyc 1330 from Micromeretics.

The thermal stability of the fibres was studied by thermogravimetric analysis (TGA) under an inert atmosphere, using a TAG 24 from Setaram. Experiments were performed on 100 mg samples held in a graphite crucible that was progressively heated at a rate of 10 °C per min to 1800 °C, under flowing high purity argon at a pressure of 100 KPa and a flow rate of 1Lh^{-1}.

2.3. Mechanical tests at high temperatures

2.3.1. Bend stress relaxation tests (BSR)

Previous studies on the thermal behaviour of ceramic fibres have shown that a bend stress relaxation test is a simple and efficient method to compare the creep resistance of several fibres and in some cases to evaluate the temperature and time dependence [31, 32].

A bending stress is applied to the fibre (which is initially perfectly straight) with a given and constant curvature R_0 and the fibre is then heat treated. After cooling, relaxation results in a residual curvature R with $R \geqslant R_0$. The stress relaxation can be quantified in terms of the parameter m which is defined as:

$$m = 1 - \frac{R_0}{R} \quad (2)$$

For a given temperature and duration, heat resistant fibres are characterized by m values close to $m = 1$ ($R \gg R_0$) while m is close to $m = 0$ ($R \approx R_0$) for compliant fibres.

2.3.2. Creep tests at high temperature under argon

The creep tests were carried-out on single fibre samples of about 160 mm in length. The ends of the filament were glued onto alumina rods with a refractory cement. Its diameter was measured by laser interferometry. In order to minimize the variations of the applied stress along the fibre, only fibres with a constant diameter within the tested length have been submitted to creep tests. The creep apparatus, designed by R. Bodet *et al.* has been described elsewhere [25, 29]. The fibre is held at the bottom of the creep apparatus and connected to the extremity of an horizontal lever (Fig. 1). The other end of the lever is locked to the axis of an inductive displacement transducer, which records the elongation of the fibre. The system is equilibrated and the load (which is calculated from the desired stress and the diameter of the fibre) is applied in the axis of the fibre.

In addition, some modifications have been implemented in order to improve the true creep elongation recording: an externally controlled air tight translation system allows the application or the release of the load. The stress can thus be applied immediately that the testing temperature is achieved.

The chamber is first evacuated with a turbomolecular pump. When a good enough vacuum is achieved

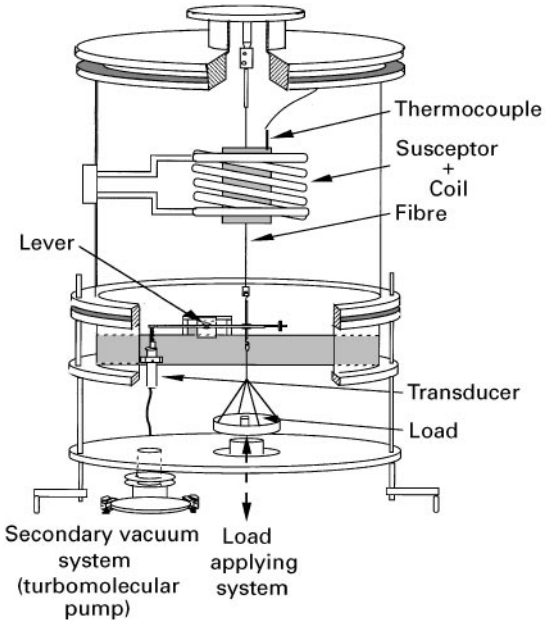

Figure 1 Creep testing apparatus for monofilaments (from [25]).

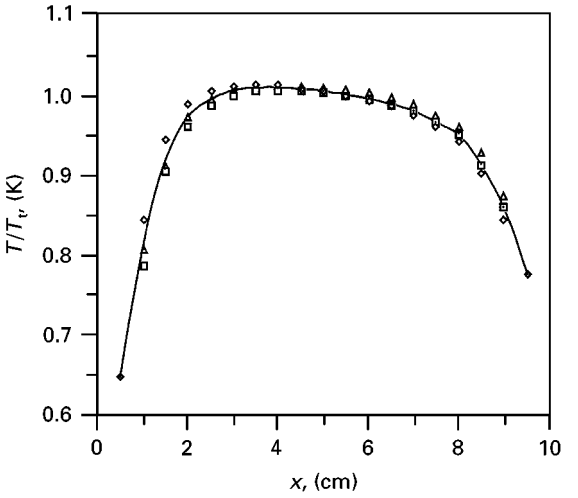

Figure 2 Temperature profiles along the fibre axis for creep tests, as a function of testing temperature T_t (temperatures T (K); (△) 1473, (□) 1573 and (◇) 1673).

($P \leqslant 10^{-5}$ Pa), the chamber is filled with high purity argon ($P = 10^5$ Pa). The fibre is then heated with a radio frequency furnace whose susceptor is a graphite cylindrical tube set around the fibre. Thermal profiles were recorded along the axis of the fibre for several testing temperatures (T_t) (Fig. 2). The heating rate was high (70 °C min^{-1}) and the stress was applied immediately after T_t was achieved, in order to avoid a structural evolution or a prior creep deformation of the fibre during heating.

The tests were performed in the range $1000 < T_t < 1600$ °C and $0.5 \leqslant \sigma \leqslant 1$ GPa. Two kinds of tests have been performed: (i) classical creep tests involving a fast heating at T_t and a temperature plateau up to the rupture of the fibre (Fig. 3a) and (ii) creep tests involving a series of plateau at increasing T_t values, recorded on the same fibre (Fig. 3b). For the latter tests, the duration of each temperature plateau was chosen in order to record, for each T_t value, the steady state creep strain. The main advantage of these tests is that the variations of the creep rate with T_t can be investigated for a given fibre and stress.

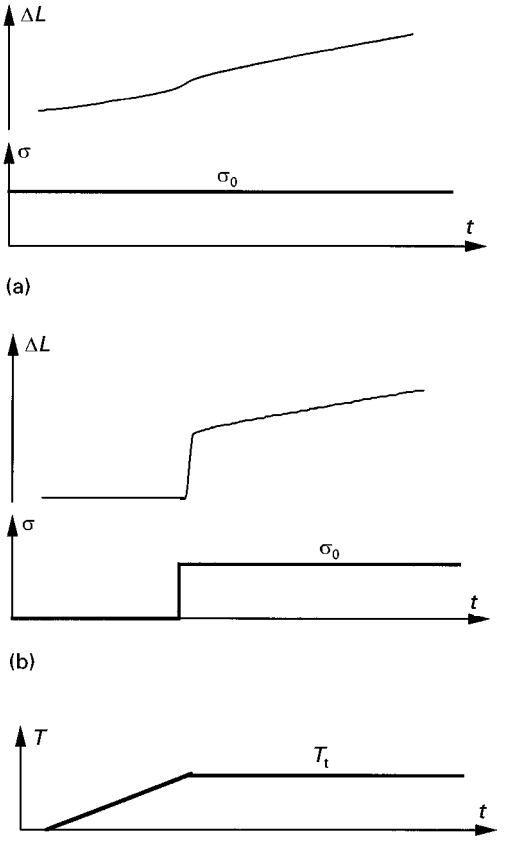

Figure 3 Elongation curves of the fibre as a function of temperature, time and applied stress, (a) the stress is applied during heating, (b) the stress is applied when the testing temperature (T_t) is just raised.

2.3.3. Tensile tests at high temperature

Tensile tests at high temperatures ($T \leqslant 1450$ °C) in air have been performed in order to characterize the strength and stiffness of the fibres as a function of temperature (T_t). Considering the short duration of the test (the fibre is tensile-tested immediately after the testing temperature is achieved, i.e., 1–2 min), the oxidation and the annealing of the fibres are not thought to strongly affect the mechanical properties of the fibre.

A tensile testing method using "hot grips" has two potential disadvantages: (i) a chemical reaction between the cement and the fibre that might result in a decrease of the fibre strength and (ii) the creep deformation of the cement which alters the recording of the fibre deformation. As a consequence, a cold grip tensile testing system has been preferred in this work.

The testing apparatus used for the tests is that developed by Villeneuve *et al.* [33] with the exception of the heating system. The fibres are heated with a platinum-resistance furnace, maintained at the testing temperature T_t that surrounds the fibre when mounted on the tensile apparatus (Fig. 4). The end the fibres were glued to the grips (small alumina rods) with a refractory cement. The total gauge length L_0 was

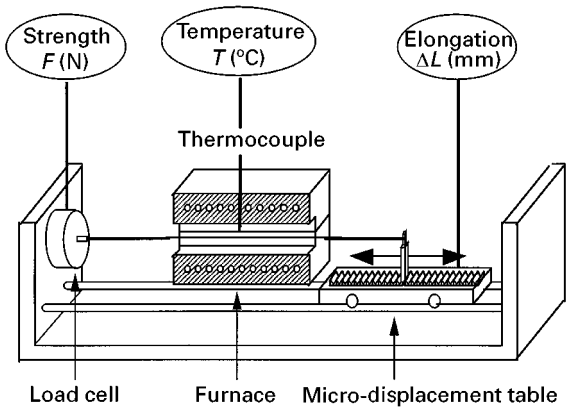

Figure 4 Tensile testing apparatus for monofilaments.

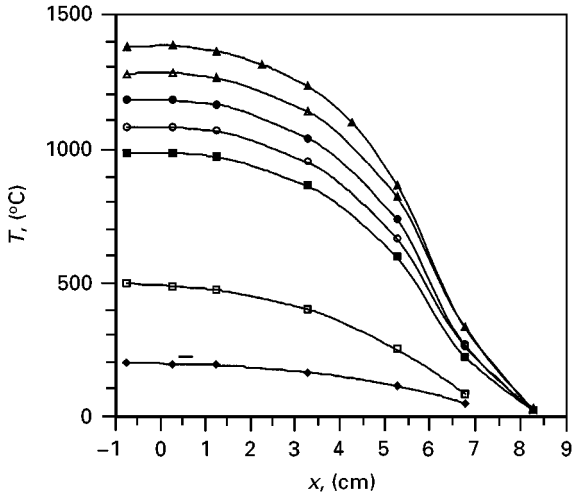

Figure 5 Temperature profiles along the fibre axis for tensile tests, as a function of testing temperatures of (◆) 200 °C, (□) 500 °C, (■) 1000 °C, (○) 1100 °C, (●) 1200 °C, (△) 1300 °C and (▲) 1400 °C.

about 200 mm so that the grips remained outside the furnace, and thus stayed cool. In the creep tests, thermal profiles were recorded for several testing temperatures (Fig. 5). The elongation rate was 1 mm min^{-1}.

3. Results and discussion

3.1. Chemical and structural properties of the as-received and heat-treated fibres

The chemical and structural characterization of the fibres of both the as-received and heat treated states, has been published elsewhere [30]. Only the main conclusions will be recalled here for the purpose of the discussion.

The chemical analysis of the fibres by EPMA shows that the chemical composition is almost unchanged after a heat-treatment under argon at temperatures up to 1800 °C. It is closed to: Si : 41.0 at %; C : 58.1 at % and O : 0.9 at %. The Hi-Nicalon fibre has a very low oxygen content and an excess of free carbon ($\approx$17 at %). As a result of the very low oxygen content (almost nil), this fibre can be considered as a SiC + C mixture which is known to be thermodynamically stable up to $\approx$2500 °C (the SiC decomposition temperature into $Si_{(1)}$ and $C_{(s)}$). A slight decomposition nevertheless takes place at very high temperatures, resulting in a silicon depletion of the fibre, initially at the surface ($T_p = 1600$ °C) and then gradually reaching into the core ($T_p \geqslant 2000$ °C). This feature is consistent with the occurrence of a pressure of gaseous silicon that has been detected by a Knudsen mass spectroscopic study on SiC + C mixtures [34]. It could also be related to an active oxidation phenomenon, due to the occurrence of traces of residual oxygen in the annealing furnace atmosphere or resulting from the decomposition of the fibre into traces of gaseous silicon monoxide ($SiO_{(g)}$).

In the as-received state, the Hi-Nicalon fibre consists of β-SiC crystals ranging in size from 2–15 nm, as compared to the 1–4 nm reported for the Si–C–O fibre [15, 17]. The free carbon is also better organized in the Si–C fibre than in the Si–C–O fibre. The carbon layers are about 2–3 nm long throughout the fibre and the number of stacks is commonly 5–8 (Fig. 6a). The carbon domains form an intergranular network and are frequently observed to sit flat on SiC crystals forming open cages. After a $T_p = 1400$ °C heat-treatment, a slight SiC grain growth is observed. The crystal now reaches a maximum size of 18–25 nm. More punctuated β-SiC rings are observed on the SAD pattern, indicating the presence of larger-size crystals. Stacking faults are also observed and in addition joined-crystals are sometimes noticed. The free carbon is also better organized than in the as-received fibre. The number of stacks is nearly the same whereas the extent

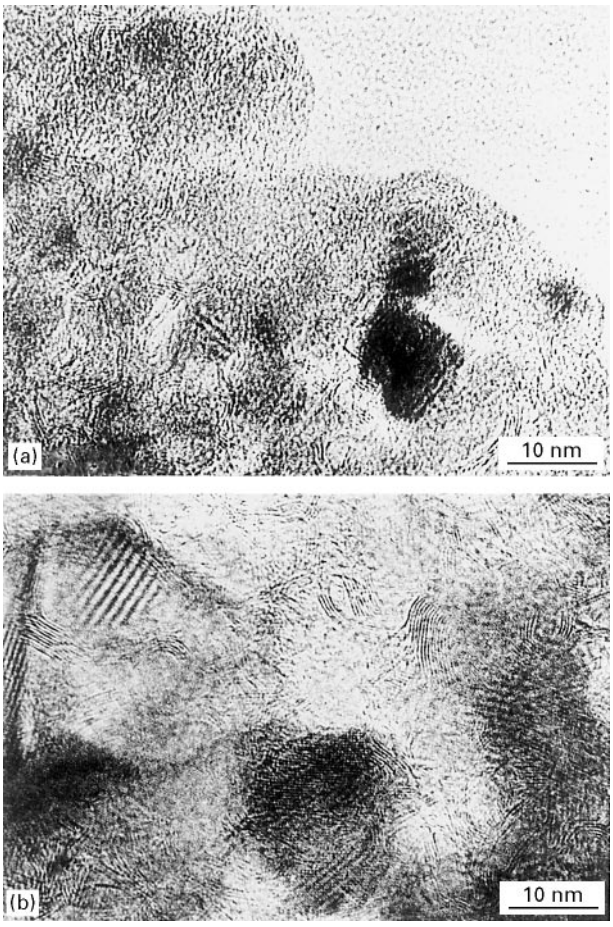

Figure 6 Lattice fringe imaging of (a) as-received Hi-Nicalon fibre and (b) annealed 1 h at $T_p = 1600$ °C under argon.

of the carbon layers is slightly larger (L_a = 3–6 nm). For $T_p = 1600\,^{\circ}C$, the maximum SiC grain size reaches $\approx$ 50 nm and joined crystals are more frequently observed. The organization of free carbon continues to improve (Fig. 6b). The number of stacks increases, reaching N = 7–12, as well as the extent of the carbon domains (L_a), with L_a = 5–10 nm.

An XRD pattern of the as-received Hi-Nicalon fibre shows three main peaks assigned to the (1 1 1), (2 2 0) and (3 1 1) Bragg reflections of the β-SiC phase. The β-SiC grain size calculated from the Scherrer equation is about 5 nm. Despite the evidence of free carbon, no peak assigned to turbostratic carbon could be observed in the pattern. The grain size is about 10 nm for $T_p = 1600\,^{\circ}C$ (t_p = 1h) and 20 nm for $T_p = 2000\,^{\circ}C$. An increase of the annealing treatment duration (t_p) also results in a SiC coarsening (Fig. 7).

The nanotexture of the Hi-Nicalon fibre is thus very different from that of the Si–C–O fibre. β-SiC crystals are larger and the free carbon phase is better organized. Free carbon can be described as a discontinuous intergranular network in the Si–C fibre whereas it was observed as isolated BSU's embedded into the SiO_xC_y continuum in the Si–C–O fibre. Heat treatments at increasing temperature (T_p) result in a gradual SiC crystal growth as well as a better organization of the free carbon phase. The structural and textural evolution with T_p nevertheless remains moderate with respect to that of the Si–C–O fibre [17–20], and displays a much better thermal stability.

The higher value of density of the Si–C fibre with respect to the Si–C–O fibre (respectively 2.77 $g\,cm^{-3}$ and 2.56 $g\,cm^{-3}$), can be assigned to the absence of the SiO_xC_y phase (a low density material) and to the better crystalline state of both the SiC and free carbon phases. Annealing treatments at increasing temperatures result in a densification of the fibres (Fig. 7). The density increase starts at about 1400 °C and progressively improves as both the temperature and hold duration are raised.

TGA experiments have shown that there is no weight change up to 1200 °C and that a slight weight loss occurs between 1200–1400 °C. Beyond 1600 °C, the decomposition rate gradually increases up to 1800 °C. The progressive weight-loss occurring at high temperature (> 1600 °C) is a consequence of the decomposition of the fibre, resulting in a silicon depletion, as has already been shown by chemical analysis.

3.2. Mechanical behaviour at high temperature of the as-received and heat-treated fibres

3.2.1. Bend stress relaxation tests

3.2.1.1. The as-received fibre. The evolution of the m parameter as a function of T_p for Si–C–O fibres (Nicalon NL202), as received and heat-treated Hi-Nicalon fibres (1600 °C/1h/Ar) is shown in Fig. 8. The results obtained for the Si–C–O fibres are in good agreement with those reported by other authors [32]. A residual strain is observed after BSR testing at a temperature as low as 1100 °C for the Hi-Nicalon fibres. The Si–C fibre has a better thermal behaviour from the BSR resistance point of view than does the

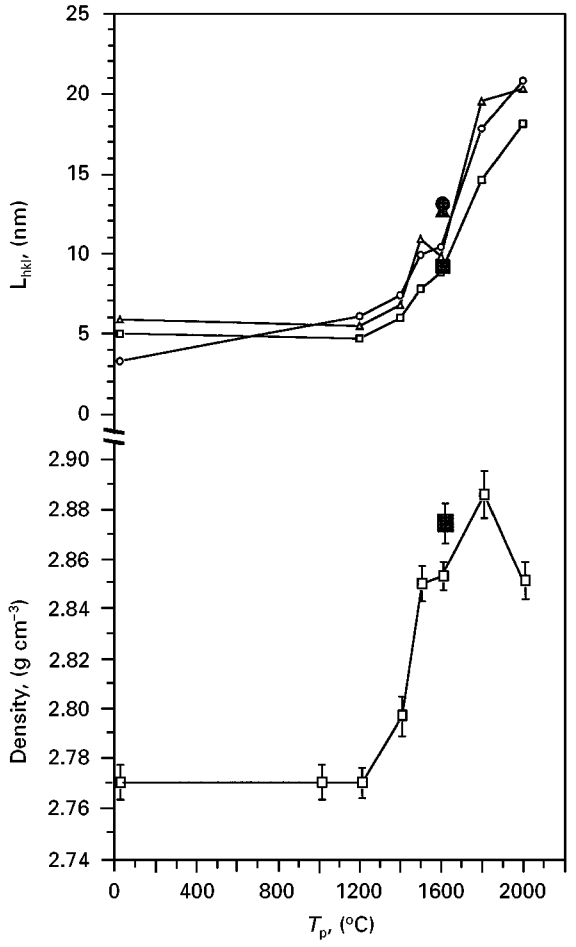

Figure 7 β-SiC crystallites apparent size and density of Hi-Nicalon fibres as a function of annealing temperature under argon (100 kPa) for (□) L111 (1 h), (△) L220 (1 h), (○) L311 (1 h), (■) L111 (10 h), (▲) L220 (10 h) and (●) L311 (10 h).

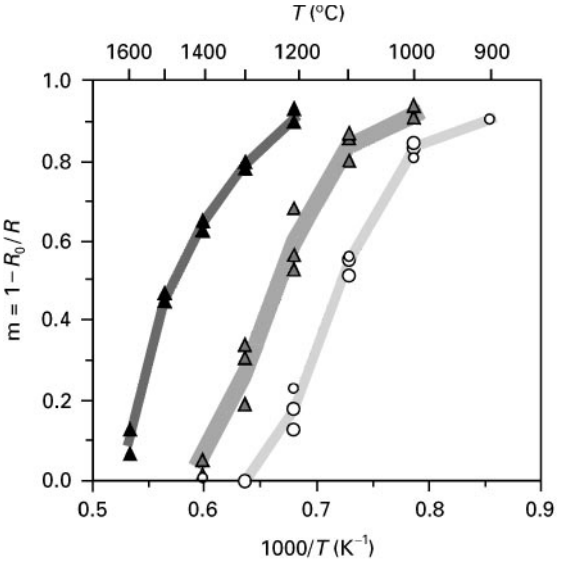

Figure 8 Stress relaxation ratio versus reciprocal pyrolysis temperature (100 kPa, t_p = 1 h) (○) Nicalon NL202 from our work (○) NL202 from Tressler *et al.* (▲) Hi-Nicalon as received and (▲) Hi-Nicalon heat treated 1600/1 h/Ar.

Si–C–O fibre since that, for a given heat treatment, the residual strain recorded for the Si–C fibres remains lower than for a Si–C–O fibre. The degradation of the mechanical properties of the Si–C–O fibre at high temperatures is attributed to the presence of the silicon oxycarbide phase which surrounds the SiC crystals. When submitted to strain or stress, this amorphous phase undergoes viscous flow at a relatively low temperature ($\geqslant 1000\,^{\circ}C$), and, as a consequence, is subject to creep strain and stress relaxation. The large decrease of the oxygen content and thus of the amorphous SiO_xC_y phase, results in an improved stress relaxation resistance at high temperatures. In fact, with respect to the Si–C–O fibre, the thermal behaviour of the stress relaxation parameter (m) for the Hi-Nicalon fibre is improved by 150 °C.

3.2.1.2. The fibre heat-treated for 1h at 1600 °C. A previous heat-treatment clearly improves the BSR thermal resistance of the fibre (Fig. 8) by about 200 °C, with respect to the as-received fibre. The structural evolution of the fibre which has been described in Section 3.1 (crystallization of the SiC phase, organization of free carbon and densification of the fibre) strongly affects the fibres capacity for flowing in a viscous manner when it is strained at a high temperature.

The influence of time and initial strain has not been studied in the present work. It should be noted that the BSR test is not a fully satisfactory method for characterizing the creep behaviour of ceramic fibres. The maximum strain level which is applied to the fibre is very low and the mechanisms responsible for the visco-elastic flow during the test are probably those involved for primary creep, rather than for steady state creep in a classical tensile creep test (see section 3.2.2). As a consequence, in the present work, the BSR test must be considered only as a qualitative and comparative thermal analysis of the fibre.

3.2.2. Creep tests

3.2.2.1. The as-received fibre. The measurement system allows a brief application of a stress on to the fibre which is maintained at the testing temperature, and it allows measurement of (i) the elastic strain, (ii) the primary creep strain and (iii) the steady-state creep strain (if any), up to rupture (Fig. 3b). If the stress is applied before the testing temperature is achieved, a strain can be recorded during heating. This may result in an under-estimation in the creep strain measurement, especially for high temperatures ($T_t \geqslant 1400\,^{\circ}C$) (Fig. 3a).

The elongation measurements as a function of time for a given stress of $\sigma = 1$GPa and for testing temperatures ranging between 1200–1600 °C are shown in Fig. 9. Generally speaking, an increase in the testing temperature results in a larger elongation rate and a decrease of time to rupture. A steady state creep domain (stationary elongation rate) is always observed for $T_t \leqslant 1400\,^{\circ}C$. For higher testing temperatures ($T_t \geqslant 1500\,^{\circ}C$) the elongation rate continuously decreases up to the rupture.

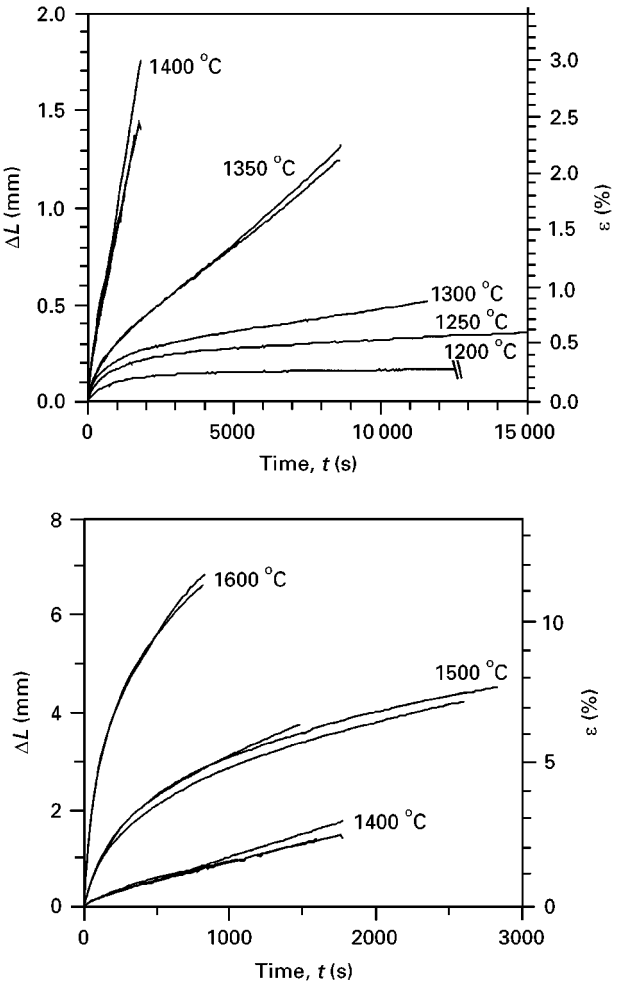

Figure 9 Elongation and calculated strain versus time for Hi-Nicalon fibres, as a function of testing temperature T_t. The applied stress is 1 GPa.

The fibres that were submitted to a series of plateau at increasing T_t values also show a primary and secondary creep behaviour up to $T_t = 1350\,^{\circ}C$ (Fig. 10). Corresponding elongation rates have been determined beyond $T_t = 1000\,^{\circ}C$ for $\sigma = 1$ GPa and beyond $T_t = 1300\,^{\circ}C$ for $\sigma = 0.5$ GPa. The thus obtained values are in good agreement with those determined according to classical tests. This feature correlates with the fact that at low temperatures ($T \leqslant 1350\,^{\circ}C$), the creep history (the prior creep tests at lower temperatures) does not affect the elongation rate with respect to those directly measured with a classical creep test. On the other hand, for $T_t \geqslant 1400\,^{\circ}C$, the steady-state creep domain is shorter and the elongation rate is lower than that measured for classical tests. The creep history would lead, in this case, to a viscosity increase of the fibre, probably due to microstructural changes induced by high temperatures and/or stress.

In order to assess the contribution of the temperature to the measured fibre strain (for instance a possible volume change), similar tests were carried-out with a very low applied stress ($\sigma = 0.1$ GPa), for $1100 \leqslant T_t \leqslant 1350\,^{\circ}C$ (Fig. 10). No strain rate is recorded during the isothermal durations except for $T_t \geqslant 1300\,^{\circ}C$, where a thermally activated shrinking of the fibre, is observed.

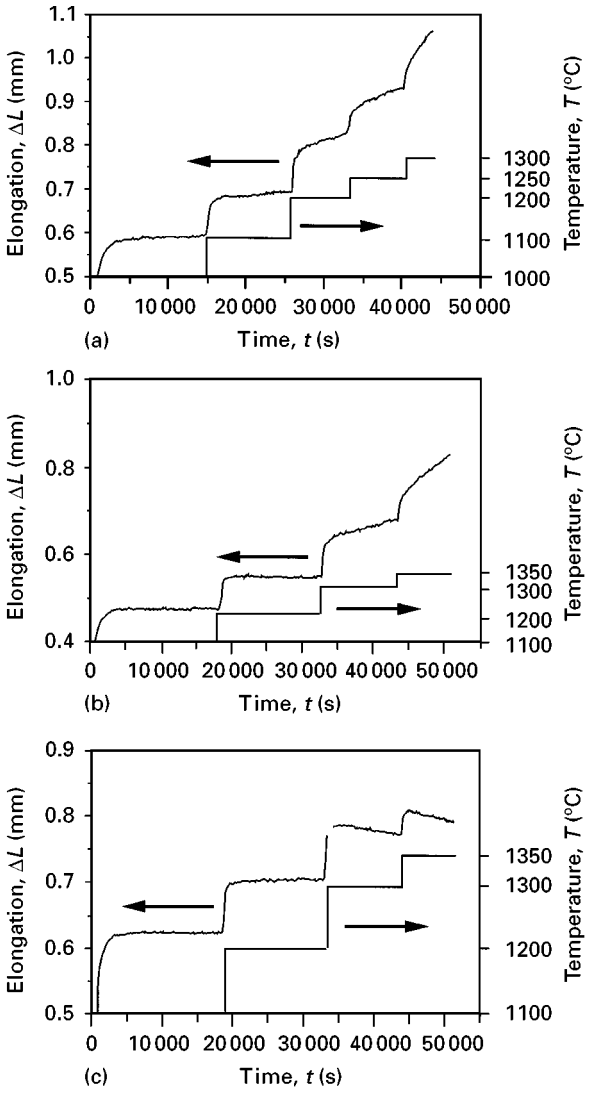

Figure 10 Elongation versus time for Hi-Nicalon fibres, as a function of applied stress and temperature. The applied stress was (a) 1 GPa, (b) 0.5 GPa and (c) 0.1 GPa.

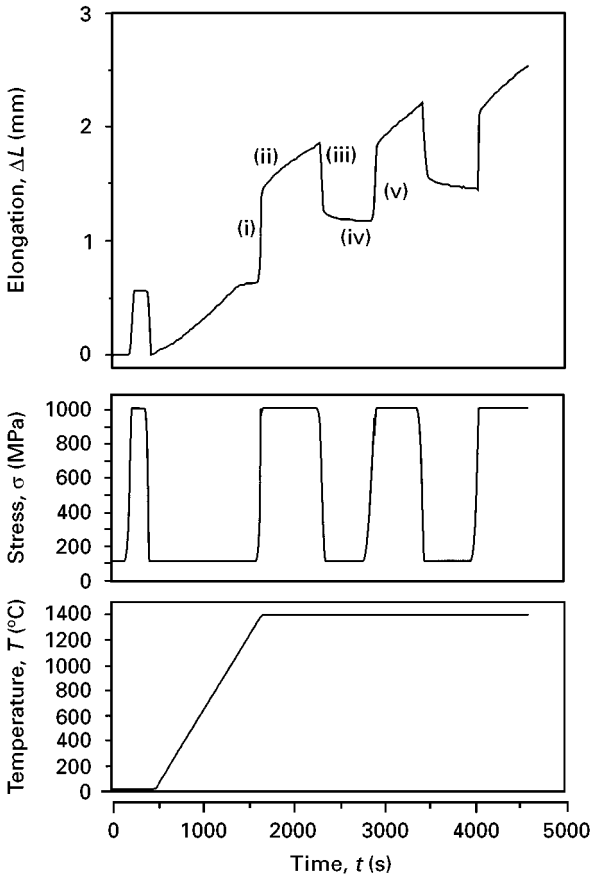

Figure 11 Creep cycling tests: elongation curves of the fibre as a function of temperature, time and applied stress.

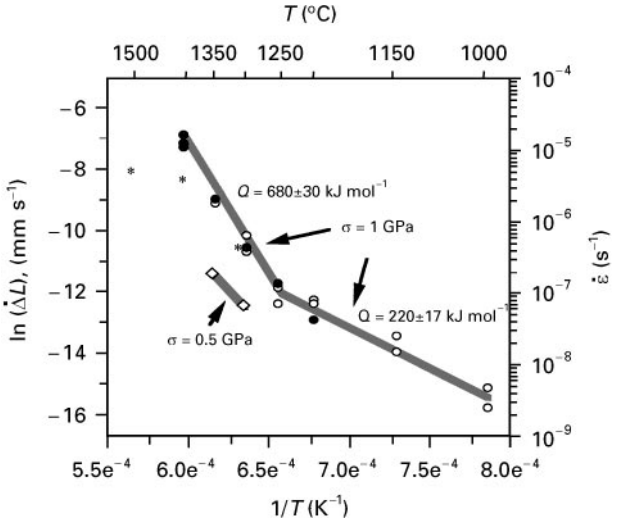

Figure 12 Steady state elongation rate as function of reciprocal testing temperature and calculated strain rate temperature dependence of as-received (○; ●) and annealed (1600 °C/1 h/Ar)(*) Hi-Nicalon fibres. The solid circles represent a single T_t dwell and the empty circles an increasing T_t dwell.

Interrupted creep tests were also performed, these consisted of a cyclic loading (alternations of $\sigma = 0.1$ and $\sigma = 1$ GPa), for $T_t = 1400\,^{\circ}C$. As is shown in Fig. 11, the deformation of the fibre includes successively: (i) the first-loading elastic strain, (ii) the constant loading creep curve (including primary and steady state domains), (iii) the first-unloading elastic strain, (iv) the time-dependant recovery, (v) the second-loading elastic strain, etc. One should note that, the first-loading elastic strain is larger than the following recorded elastic strains (whether loading or unloading), which is consistent with a stress-induced stiffening of the fibre. However, after creep deformation and unloading, the recovery domains are incomplete which results in a permanent deformation of the fibre. These characteristics suggest a visco-plastic strain of the fibre (steady-state creep domain and permanent deformation) as well as a visco-elastic component (recovery).

For constant testing temperatures and a given applied stress of $\sigma = 1$ GPa, the steady state creep elongation rate (ΔL_{oT}), plotted in an Arrhenius diagram (Fig. 12) shows two distinct linear domains, corresponding to two different apparent activation energies (Q_{ap} and Q'_{ap}). For $1000 \leqslant T_t \leqslant 1250\,^{\circ}C$, Q_{ap} is equal to $220\,kJ\,mol^{-1}$ while for $1250\,^{\circ}C \leqslant T_t \leqslant 1400\,^{\circ}C$, the phenomenon is far more sensible to the temperature effect ($Q'_{ap} = 680\,kJ\,mol^{-1}$).

The steady-state creep elongation rate values have been used to infer (i) the true activation energy (Q) for the creep mechanism, (ii) the effective gauge length

(L_{OT}) for each T_t value, and (iii) the steady-state creep strain rate ε_{oT} (see Appendix I) (Fig. 12). In addition, the complete creep curves $\varepsilon_T = f(t)$), including both primary and secondary creep domains have been calculated from the elongation curves and the L_{OT} values (Fig. 9).

The activation energy, inferred from the thermal variations of the steady-state creep strain rate for an applied stress of 1 GPa, are respectively:

$$Q = 220 \pm 17\ \text{kJ mol}^{-1} \text{ for } 1000 \leqslant T_t \leqslant 1250\ ^\circ\text{C}$$

$$Q' = 700 \pm 30\ \text{kJ mol}^{-1} \text{ for } 1250 \leqslant T_t \leqslant 1400\ ^\circ\text{C}.$$

3.2.2.2. Heat treated fibres under argon. The creep behaviour of heat treated fibres under argon at temperatures of (1400 and 1600 °C) have also been characterized. The creep curves for the as-received and heat treated fibres are shown in Fig. 13, for a testing temperature of 1400 °C and an applied stress $\sigma = 1$ GPa.

Similarly to the as-received fibres, all the creep curves contain a steady state creep domain, whatever the heat-treatment temperature. It is clear that the steady state creep strain rate decreases when T_p is increased. The time to rupture of fibres that had been previously heat-treated at a temperature of 1400 °C is increased, while it is significantly reduced for a heat treatment at 1600 °C.

The creep curves for as-received and heat treated fibres (1600 °C/1 h/Ar) as a function of testing temperature ($1200 \leqslant T_t \leqslant 1500$ °C) are shown in Fig. 14, for an applied stress $\sigma = 1$ GPa. The strain recorded for heat treated fibres remains considerably smaller than that of the as received fibre, for all the tested temperatures. This is especially true for high temperatures ($T_t = 1400$–1500 °C). It is noteworthy that when heat-treated at 1600 °C, the fibre exhibits a steady-state creep domain up to a testing temperature $T_t = 1500$ °C, while the creep rate of the as-received fibre continuously decreased up to the rupture at that temperature.

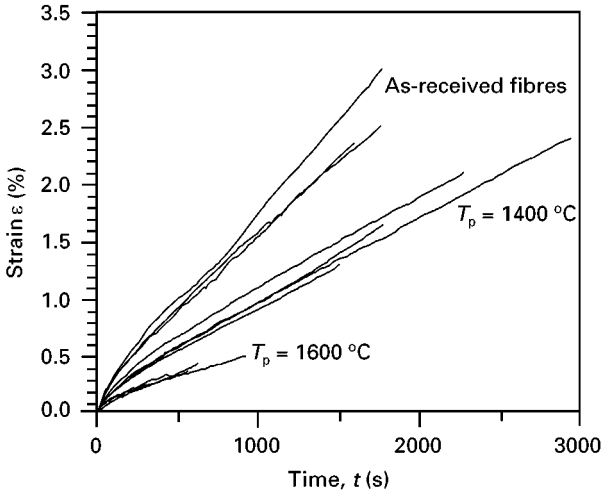

Figure 13 Annealing effect on the strain of Hi-Nicalon fibres. Pretreatment under argon (100 kPa), $T_p = 1400$–1600 °C, $t_p = 1$ h. Creep tests under argon at $T_t = 1400$ °C, the applied stress is 1 GPa.

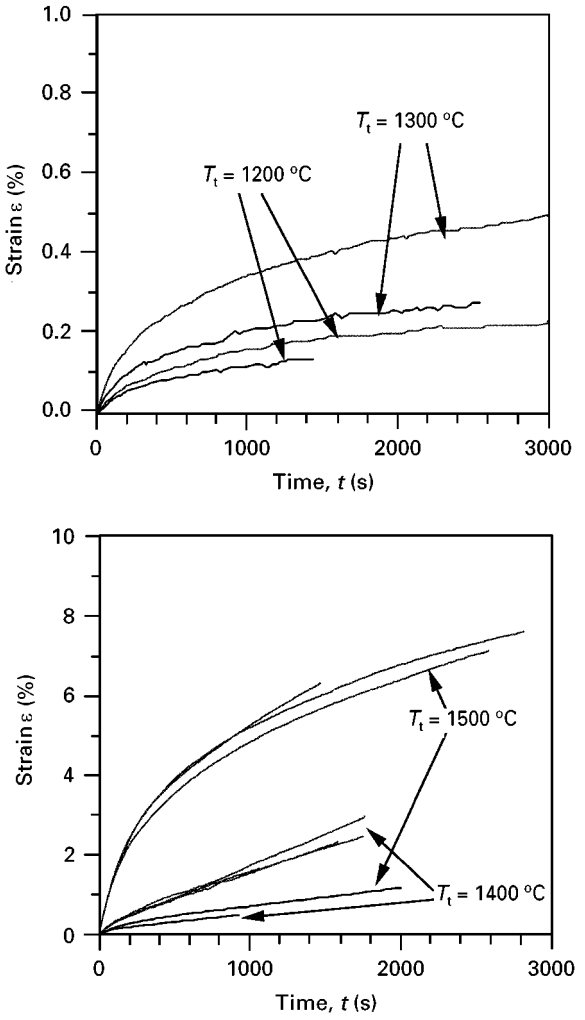

Figure 14 Annealing effect upon the strain of Hi-Nicalon fibres and as received fibres treated under argon (100 kPa), $T_p = 1600$ °C, $t_p = 1$ h. Creep tests under argon at $T_t = 1200$–1500 °C, applied stress is 1 GPa.

From the results obtained for pyrolysed fibres, it is clear that the annealing treatment induces a marked stabilization of the mechanical properties, in terms of creep at high temperatures. The structural and textural changes that were described in Section 3.1 result in an increase of the viscosity of the fibre at high temperatures and, as a consequence, in a decrease of the creep strain rate, for a given stress and testing temperature. Furthermore, a previous heat-treatment also has a structural stabilization effect during the creep test at high temperature. Unlike the untreated fibre case, the fibres that were heat-treated at a temperature of 1600 °C are not expected to undergo any structural change during the test up to $T_t = 1500$ °C. As a consequence, the steady state creep behaviour of the heat-treated fibre is still observed for $T_t = 1500$ °C.

3.2.3. High temperature tensile tests

3.2.3.1. The as-received fibre. The tensile strength (σ^R) and the Young's modulus (E) of the as-received fibre have been determined at ambient under the same conditions as those for the high temperature tests (gauge length $L_0 = 200$ mm, elongation rate

$v = 1\,\text{mm}\,\text{min}^{-1}$). The stress–elongation curves (Fig. 15a) show typical brittle behaviour. The Young's modulus of the fibre is higher than that of the Si–C–O fibre (280 GPa versus 200 GPa for the Si–C–O fibre). Despite of the important gauge length, the tensile strength is relatively high ($\sigma^R = 2500$ MPa).

When tested at high temperature ($T_t = 1400\,^\circ\text{C}$), three main features are noticeable: (i) σ^R significantly decreases (Table I), (ii) the stress–elongation curve shows a marked non-linear behaviour (Fig. 15b) and (iii) the stiffness of the fibre, measured within the linear domain for a low elongation state, is also severely affected by temperature (Fig. 15b). A slight increase in the testing temperature ($T_t = 1450\,^\circ\text{C}$) emphasises these three characteristics (Fig. 15c). Furthermore, a decrease of the elongation rate enhances the apparent visco-plastic behaviour (Fig. 15c). This feature is confirmed by cycling tests at $T_t = 1450\,^\circ\text{C}$ (series of loading–unloading).

Each cycle induces an additional residual elongation of the unstressed fibre, which rapidly decreases during the first two cycles up to a constant value (Fig. 16a). The stiffness of the fibre also varies during the cycling test. A slight increase of the stiffness is measured between the first and second cycles (the stress–elongation ratio is about 5% higher for the second cycle).

Finally, a "pseudo"-stress-relaxation test has been performed. It consisted of measuring the evolution of the stress resulting from the fixed elongation state of the non-isothermal fibre. The marked visco-plastic

TABLE I Tensile strength at ambient and high temperature in air for as-received and annealed Hi-Nicalon fibres

	As-received			1600/1h/Ar
	Ambient	$T_t = 1400\,^\circ\text{C}$	$T_t = 1450\,^\circ\text{C}$	$T_t = 1450\,^\circ\text{C}$
σ^R(MPa)	2630	1510	1290	1030
Stand. dev. (MPa)	370	120	230	90

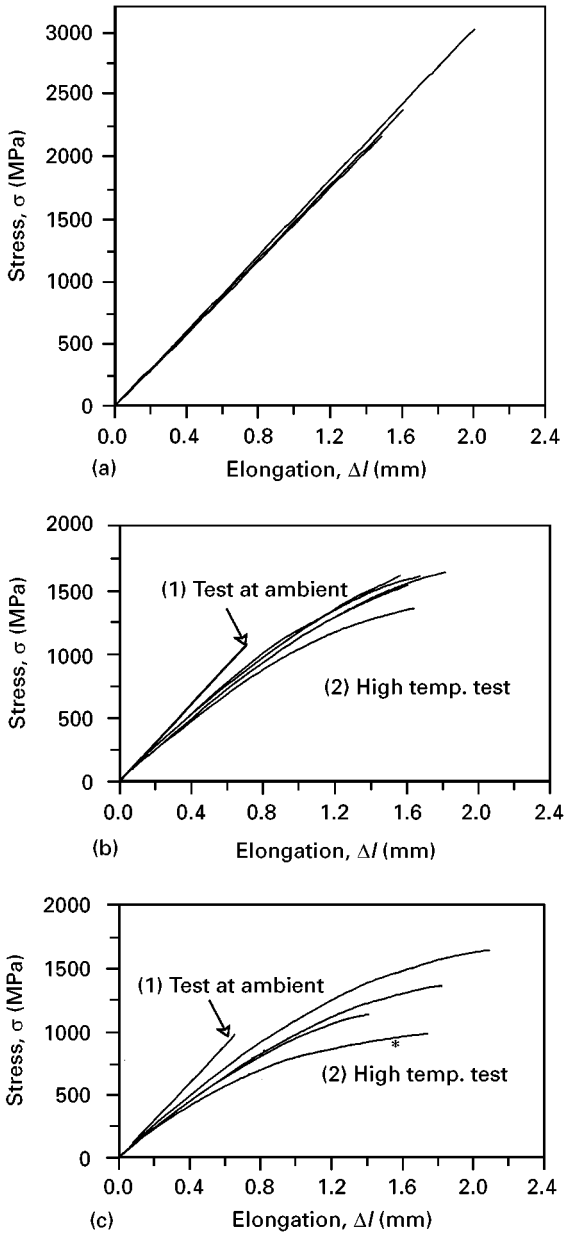

Figure 15 Stress/elongation curves in air at high temperature for Hi-Nicalon fibres (cold grips). The conditions were (a) Ambient, $L_o = 200$ mm and $v = 1$ mm per min, (b) 1400 °C in air $L_o = 200$ mm, $v = 1$ mm per min and (c) 1450 °C in air, $L_o = 200$ mm, $v = 1$ mm per min except the trace marked (*) $v = 0.25$ mm per min.

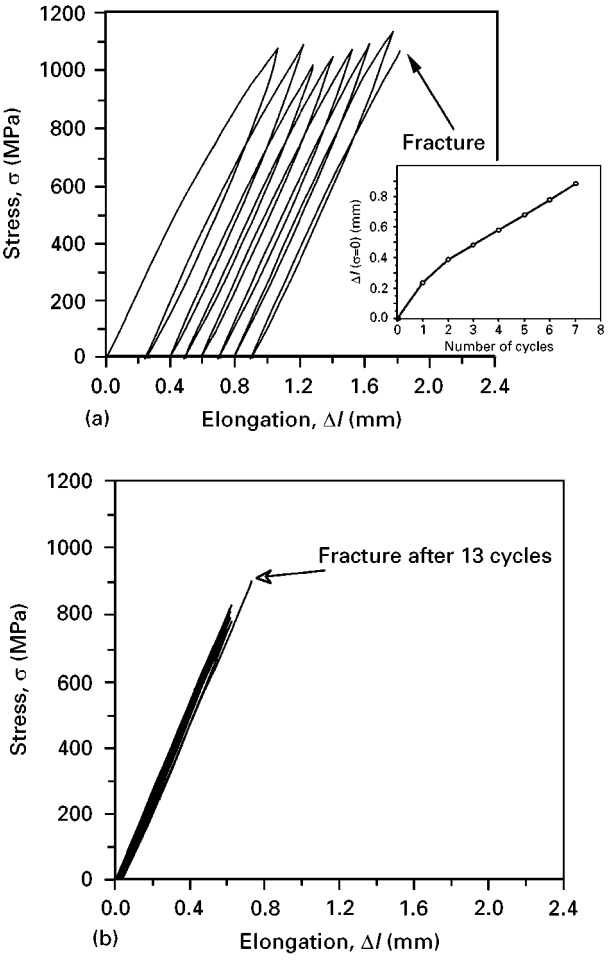

Figure 16 Cycling stress/elongation curves at 1450 °C in air. (a) as received Hi-Nicalon fibre (insert: residual elongation of the unstressed fibre as a function of the number of cycles), (b) annealed Hi-Nicalon fibre (1600 °C/1 h/Ar). For both fibres $L_0 = 200$ mm and $v = 1$ mm per min.

behaviour at high temperature is also responsible for a low stress relaxation resistance (Fig. 17a). The stress ($\sigma \approx 1000$ MPa) rapidly vanishes with time (it is reduced by 50% for $t \approx 400$ s).

3.2.3.2. The heat-treated fibre. The stress–elongation curves for the heat-treated fibres ($T_p = 1400$ and $T_p = 1600\,^{\circ}C$) show modified characteristics with respect to the untreated fibre:

(i) when tested under the same conditions, the tensile strength of the fibres annealed at $T_p = 1400\,^{\circ}C$ is slightly higher than that for the as-received fibres, whilst it strongly decreases for $T_p = 1600\,^{\circ}C$ (Fig. 18).

(ii) the visco-plastic behaviour of the as-received fibre is reduced after annealing at $1400\,^{\circ}C$ (Fig. 18(a and b)) and has almost disappeared at $T_p = 1600\,^{\circ}C$ (Fig. 18c), with an elastic behaviour up to the rupture at $T_t = 1450\,^{\circ}C$.

(iii) the reduction in the stiffness of the fibres at high temperature is lower for the heat-treated fibres (Fig. 19).

When performed on a fibre that had been previously annealed for 1 h at $1600\,^{\circ}C$, a cycling test clearly shows that the fibre has lost its non-linear mechanical behaviour at $T_t = 1450\,^{\circ}C$ (Fig. 16b). Unlike for the untreated fibre, no significant residual strain is induced by the stress-cycling, and the stress–elongation curves remain elastic during the whole test.

A stress-relaxation test performed at $1450\,^{\circ}C$ also shows that the visco-plastic behaviour has almost vanished after a heat treatment at $1600\,^{\circ}C$ (Fig. 17b).

In order to assess the temperature effect on the stiffness of the fibres, a series of loading-unloading tests were carried out on a single fibre at increasing test temperatures. When the variations of the apparent Young's modulus (the stress–elongation ratio, divided by the total gauge length) are plotted as a function of the testing temperature T_t (Fig. 19), it is clear that the stiffness of the untreated fibre is slightly reduced from $T_t = 800\,^{\circ}C$ and strongly decreases in the range $1200 \leqslant T_t \leqslant 1450\,^{\circ}C$. On the other hand, the stiffness of the heat-treated fibres is less affected by high T_t values. It slightly decreases between $T_t = 1000$–$1300\,^{\circ}C$ for $T_p = 1600\,^{\circ}C$. A calculation of

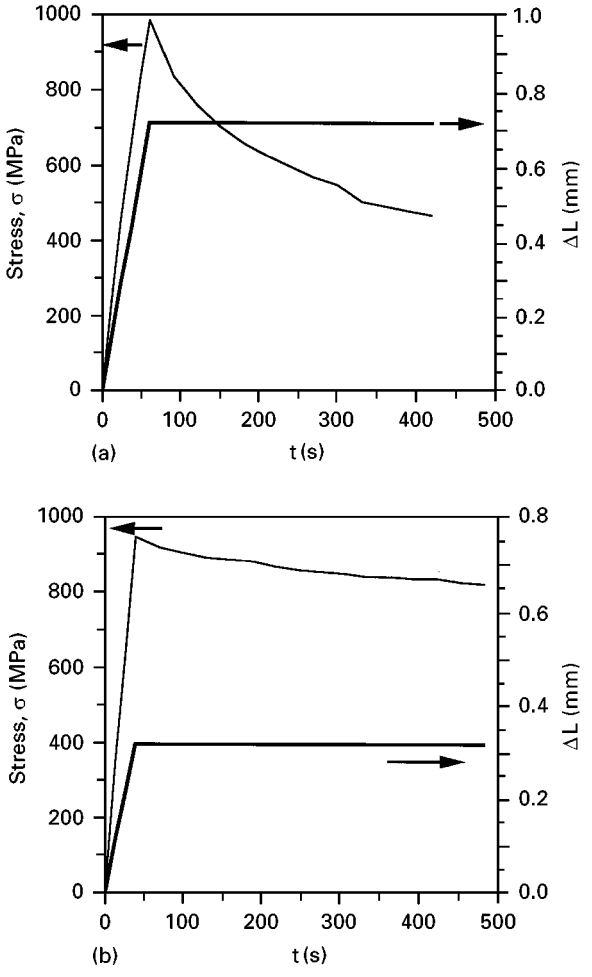

Figure 17 Stress relaxation curves at $1450\,^{\circ}C$ in air. (a) as received Hi-Nicalon fibre; (b) annealed Hi-Nicalon fibre ($1600\,^{\circ}C$/1 h/Ar)

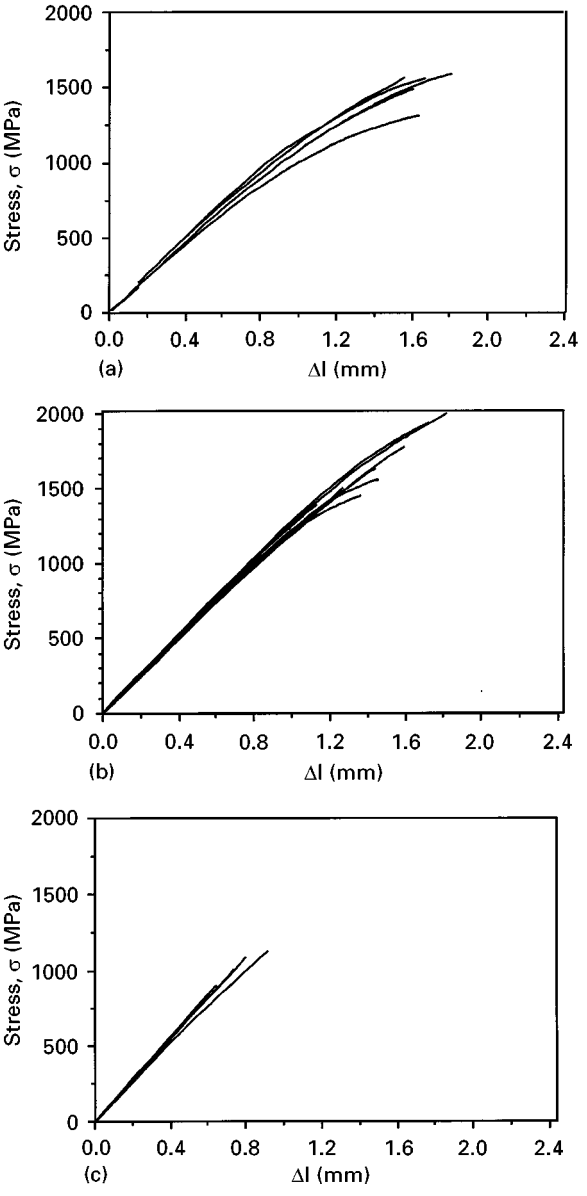

Figure 18 Stress/elongation curves in air at high temperature for annealed Hi-Nicalon fibres. The conditions used were $L_0 = 200$ mm, $v = 1$ mm per min (a) Hi-Nicalon as received tested at $1400\,^{\circ}C$/air (b) annealed at $1400\,^{\circ}C$/1 h/A_2 and tested at $1400\,^{\circ}C$/air and (c) annealed at $1600\,^{\circ}C$/1 h/A_2 and tested at $1450\,^{\circ}C$/air.

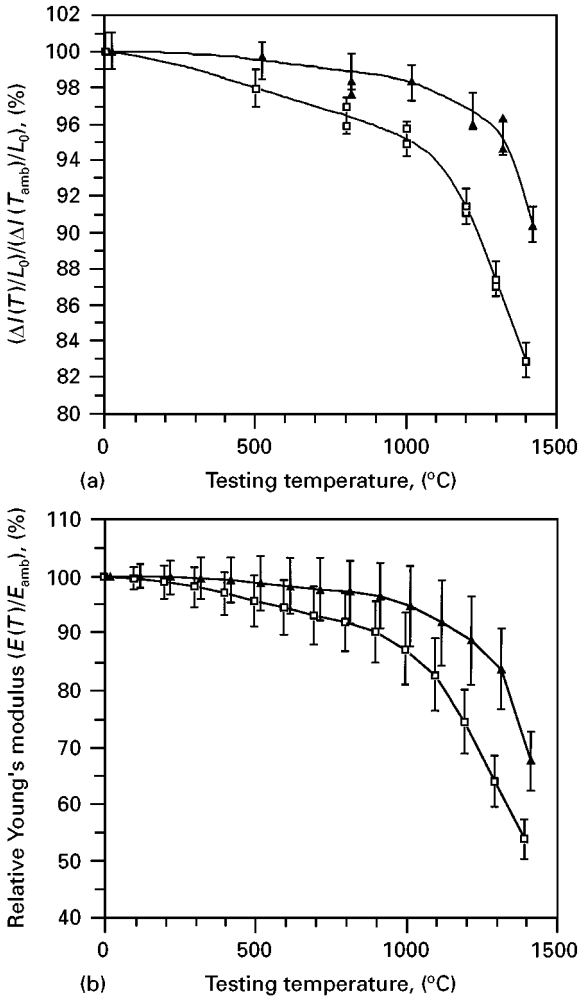

Figure 19 (a) Stress/elongation ratio and (b) calculated relative Young's modulus, as a function of testing temperature for (□) as-received and (▲) heat treated at 1600 °C Hi-Nicalon fibre.

the corrected Young's modulus, based on the temperature profiles, determined for each T_t value (developed in Appendix 2) has been performed (Fig. 19). The corrected Young's modulus is reduced by almost 45% at 1400 °C from its value at ambient for the untreated fibre and is about 35% for $T_p = 1600$ °C.

An analysis of the morphology of the fracture surface of the tensile-tested filaments at high temperature shows that the oxidation phenomenon which is expected to occur in air is very limited, due to the briefness of the test and the rather good oxidation resistance of the material. In fact, the silica layer formed at the surface of the fibre is very thin and, as a consequence, oxidation is not thought to significantly influence the mechanical behaviour at high temperature.

4. General discussion

The various chemical and structural analyses of the experimental Si–C fibre have shown that a lowering of the oxygen content results in a much improved thermal stability [30]. Nevertheless, a slight evolution with increasing T_p has been shown, which starts to occur within the range $1200 \leqslant T_p \leqslant 1400$ °C. This consists of

(i) a crystallization of the β-SiC phase for $T_p > 1200$ °C,

(ii) an organization of the free carbon phase for $T_p = 1400$ °C and

(iii) a densification of the fibre for $T_p > 1200$ °C.

On the other hand, the various mechanical tests have shown a much better thermal behaviour with respect to the Si–C–O fibre, in terms of creep, stress relaxation resistance, and tensile strength at high temperature as it has already been previously reported [29].

Nevertheless, BSR tests have clearly shown that the fibre was subjected to a viscous flow at a temperature as low as 1000 °C. In addition, for high stress levels (1 GPa), primary and steady state creep were measured for the same testing temperature. Both the creep and relaxation phenomena were observed to be thermally activated and an unexpected creep strain was reached ($\varepsilon^f \approx 12\%$) at 1600 °C, with an apparent fibre necking effect.

The drop in the thermal properties of Si–C–O fibres (visco-plastic behaviour, stiffness decrease) has already been reported by other authors [35, 36]. Such behaviour is assigned to the compliant amorphous SiO_xC_y phase surrounding the SiC crystals. This material is responsible for the low thermal resistance, as observed by (i) BSR tests [31, 32], (ii) creep tests [24, 25] and (iii) tensile tests [35].

Hi-Nicalon fibres contain very little of the amorphous SiO_xC_y phase, and as a consequence, it has a much better creep resistance than the Si–C–O fibres. Despite its very small oxygen content, creep strain is detected from a testing temperature as low as 1000 °C. In this case, the creep mechanism should not be related to the occurrence of an amorphous intergranular material.

Hi-Nicalon fibres are mainly composed of SiC nanocrystals (≈ 76 vol %) with an average size close to 5 nm. These crystals should be interconnected (with the occurrence of grain boundaries), and/or separated by the intergranular free carbon phase. The fibres also contain a secondary intergranular free carbon phase (≈ 15 vol %) that forms a continuous framework between the SiC crystals. The very low amount of oxygen atoms present may also be bonded at the surface of SiC crystals through Si–O–Si layers at the SiC/SiC interfaces (if any) and/or SiC/free carbon interfaces. In addition, one should consider the cohesion between the different phases and especially the SiC/free carbon interfaces.

Interrupted creep tests and cycling tests have shown that Hi-Nicalon fibres have a visco-plastic behaviour at high temperature. The continuity of the free carbon phase also produces a plastic behaviour in this material at high temperature. If SiC crystals are connected to each other, then a visco-plastic behaviour of the SiC phase should also be assumed, possibly produced by a grain-sliding mechanism. Finally, a weak bonding between SiC crystals and free carbon could also contribute to the plastic behaviour at high temperature.

Mechanical studies on rayon precursor based fibres at high temperatures have been performed by Bacon and Smith [37]. The texture of rayon-based fibres is

similar to that of the free carbon in the Si–C fibre, i.e., a porous material with a density of 1.4 g cm^{-3}, with a poor crystalline state (with turbostratic domains in the range of 1–10 nm and 3–4 layer stacks) [41]. Bacon and Smith reported a non-linear mechanical behaviour of the rayon-based carbon fibre, beginning at 900 °C that was enhanced with increasing temperature. The plastic behaviour is very marked for $T_t \approx 1900$ °C which is the maximum treatment temperature achieved during production (HTT). Cycling tests of the carbon fibre at 1900 °C under an inert atmosphere also revealed a thermal behaviour that is very close to that of the Si–C fibre for $T_t = 1450$ °C. The plastic behaviour of the carbon fibres takes place at a much higher temperature. Nevertheless, the mobility of the carbon domains that is required for the apparent organization of the free carbon phase of the Si–C fibre at $T_p = 1400$ °C, should also be responsible for the drop of the viscosity of the fibre at 1400 °C. Such a mechanism (rotation, dewrinkling and sliding of the carbon domains) would be aided by the high porosity of the material.

Creep deformations of the β-SiC phase should also be expected, especially if the grains are interconnected. Intergranular sliding and the blocking of grain asperities could induce normal stresses between crystals. The grain sliding and the stress-accommodating processes (for example a diffusion mechanism) would be the controlling parameter for creep. In fact, one could argue that the activation energy for self-diffusion and grain boundary diffusion of carbon ($E_{sd} = 841$ kJ mol^{-1} and $E_{gbd} = 563$ kJ mol^{-1}) and silicon ($E_{sd} = 912$ kJ mol^{-1}) in SiC [38, 39] are rather close to the value of the apparent activation energy for creep in Si–C fibres ($Q' = 700$ kJ mol^{-1}) for $1250 < T_t < 1400$ °C.

Small amounts of oxygen should also promote (i) solid transport through a diffusion process at the grain boundary and/or (ii) vapour transport due to $SiO_{(g)}$ and $CO_{(g)}$ species. Such phenomena could also account for the occurrence of plastic deformation.

The very small grain size of the SiC suggests that the SiC/free carbon interface may play a large role in the capacity of the Si–C fibre to be subjected to plastic deformation.

Considering the validity of the mechanism(s) involved for creep, the change of the thermal dependence of the creep strain rate of the fibre (change of the value of the activation energy at $T_p = 1250$ °C) appears to be difficult to explain.

With respect to the as-received fibres, notable changes in the mechanical behaviour of heat treated fibres were observed: (i) the visco-plastic behaviour is reduced for $T_p = 1400$ °C and almost vanished for $T_p = 1600$ °C, (ii) when heat-treated at $T_p = 1600$ °C, the residual strain or stiffening effect induced by cycling on the as-received fibre vanishes and (iii) the decrease of stiffness with testing temperature (T_t) becomes less significant with increasing annealing temperature.

These mechanical changes are obviously related to the evolution of the microstructure of the fibre: (i) the SiC crystal growth with T_p, (ii) the increase of the free carbon domain size in extension (L_a) and thickness (L_c), (iii) their ordering along the surface of SiC grains and (iv) the densification of the fibre, which is attributed to the free carbon intergranular material.

All these characteristics tend to decrease the propensity of the fibre to be subject to creep strain, whatever the effective mechanism involved. Heat treatments also improve the thermal stability of the fibre from a structural point of view. In fact, whilst the steady creep behaviour was only detected for $T_t \leqslant 1400$ °C for the as-received fibre, it is still observed for $T_t = 1500$ °C when the fibre has previously been heat-treated at $T_p = 1600$ °C.

In addition to a thermally-induced plastic behaviour, an apparent decrease of the stiffness of the Si–C fibre was detected at high temperatures (as observed by tensile tests and interrupted creep tests). This feature is generally associated with the appearance of anelastic behaviour at high temperature [35–37]. It has already been reported at 1200 °C in Si–C–O fibres by Pysher *et al.* who assigned this behaviour to the compliant amorphous SiO_xC_y phase [35]. The evolution of the stiffness of a rayon-based carbon fibre as a function of temperature is remarkably similar to that obtained for the Si–C fibre, but it is shifted towards higher temperatures [37].

The thermal behaviour of a material is generally strongly related to the nature and the volumetric ratio of the different constituent phases and also to the cohesion between those phases.

Only a slight evolution in the Young's modulus is reported for polycrystalline silicon carbide within the studied temperature range (a progressive decrease in stiffness is observed, reaching 5–10% at 1300 °C) [1].

The thermal behaviour of the Young's modulus for pyrolytic carbons strongly depends on the type of material tested [40–43]. On the one hand, the Young's moduli of soft carbons and graphites show (1) the presence of a maximum at a temperature below HTT and (2) a general decrease with increasing temperature above HTT. On the other hand, for hard carbons and glassy carbons a strong decrease above HTT is observed but no maximum in the elastic modulus below HTT is recorded.

Due to the nanometer size of the SiC grains within the fibre, the SiC/free carbon interface may also play a significant role in the elastic properties at high temperature. The decrease of the stiffness would be more marked as the bonding strength of the interface weakens.

5. Conclusion

The present work has shown that a Si–C fibre containing a very low oxygen content which was expected to be thermally stable was in fact, subject to a moderate structural evolution at temperatures above 1300 °C.

It has been shown that for a temperature as low as $T_t \geqslant 1000$ °C, a stressed fibre undergoes a viscous flow. This phenomenon is thermally activated, especially at $T_t \geqslant 1300$ °C (the apparent production temperature), where an increase in the creep rate temperature dependence is observed. This anomalous mechanical behaviour may be partly explained by the

structural instability of the fibre within this temperature range.

This is shown by the observation that, when the fibre is heat treated and, as a consequence, better organized (with an improved thermal stability), its visco-plastic behaviour is highly reduced in addition to its creep resistance at high temperature.

Appendix 1. Calculation of steady state creep strain and activation energy from experimental elongation measurements

During the creep test, the fibre does not experience a uniform temperature and, consequently, the creep strain is not constant along the whole tested length. As a consequence, the elongation recorded during the test does not result from the strain of an isothermal length. The calculation of strain (ε) from the measured elongation (ΔL) is not obvious.

Despite those considerations, the calculation of the steady state creep strain at a given temperature shall be investigated. It is based on the temperature profiles along the fibre axis for each testing temperature T (Fig. 2),

$$g_T(x) = \frac{T(x)}{T_t} \tag{A1}$$

and, on the other hand, on the assumption that the creep strain rate is related to temperature by the Dorn equation:

$$\dot{\varepsilon} = A.\exp\left(\frac{-Q}{RT}\right) \tag{A2}$$

where A is a pre-exponential parameter, Q the activation energy for creep, T the absolute temperature and R the gas constant. If T_t is the testing temperature, the measured elongation ΔL_{T_t} is equal to the addition of elemental elongations $dl(x)$:

$$\Delta L_{T_t} = \int_0^{L_o} dl = \int_0^{L_o} \varepsilon_{T_t}\, dx \tag{A3}$$

where L_o is the fibre length and ε_T is the elongation at the x axis.

Within the steady state creep domain, deriving Equation A3, one has:

$$\Delta \dot{L}_{oT_t} = \int_0^{L_o} \dot{\varepsilon}_{0T_t}\, dx \tag{A4}$$

If the temperature profiles along the fibre $g_T(x)$ is known for each testing temperature T_t, combining Equations A2 and A4 one finds:

$$\Delta \dot{L}_{oT_t} = A.\int_0^{L_o} \exp\left(\frac{-Q}{RT_t.g_T(x)}\right) dx \tag{A5}$$

$\Delta \dot{L}_{oT_t}$ values are measured for each testing temperature. Conversely, the pre-exponential parameter A and the activation energy Q are both unknown. To determine A and Q, it is necessary to optimize their respective values in order that the calculated elongation rates (from Equation A5) are as close as possible to their experimental values. For instance, Q can be determined according to the following procedure. Considering: (i) that the logarithm of the experimental elongation rates are linearly related to the reciprocal temperature for $1000 \leqslant T_t \leqslant 1250\,^{\circ}C$ (Fig. 12), according to the following equation:

$$\ln(\Delta \dot{L}_{oT_t}(T_t)) = \alpha - \frac{Q_{ap}}{R \cdot T_t} \tag{A6}$$

where Q_{ap} is the apparent activation energy for the experimental $\Delta \dot{L}_{oT_t}$ thermal variations, and (ii) that for a given Q value, the logarithm of the calculated elongation rates (from Equation A5) are also linearly related to the reciprocal temperature (Fig. 20)

$$\ln(\Delta \dot{L}_{oT_t}(T_t)) = \beta - \frac{Q^*}{R \cdot T_t} \tag{A7}$$

where Q^* is the apparent activation energy for the calculated ΔL_{oT_t} thermal variations. The activation energy of steady state creep strain rate Q is the solution of

$$Q^*(Q) = Q_{ap} \tag{A8}$$

The calculated true activation energy (Q), for $1000 \leqslant T_t \leqslant 1250\,^{\circ}C$, is almost the same that the experimental apparent activation energy (Q_{ap}), determined from the ΔL_{oT_t} thermal variations, with a value equal to $220 \pm 17\ kJ \cdot mol^{-1}$. One should argue that the assumption used in Equation A2 is not valid for $T_t > 1250\,^{\circ}C$ since the creep strain rate apparently obeys two distinct thermal variations (Fig. 12) ($1000 \leqslant T \leqslant 1250\,^{\circ}C$ and $1250 \leqslant T \leqslant 1400\,^{\circ}C$), associated to two activation energies. Under those conditions, the calculation of ΔL_{oT_t} according to Equation A4 must take into account the assumption of two successive Dorn equations for creep strain rate:

$$\dot{\varepsilon} = A.\exp\left(\frac{-Q}{RT}\right) \tag{A2}$$

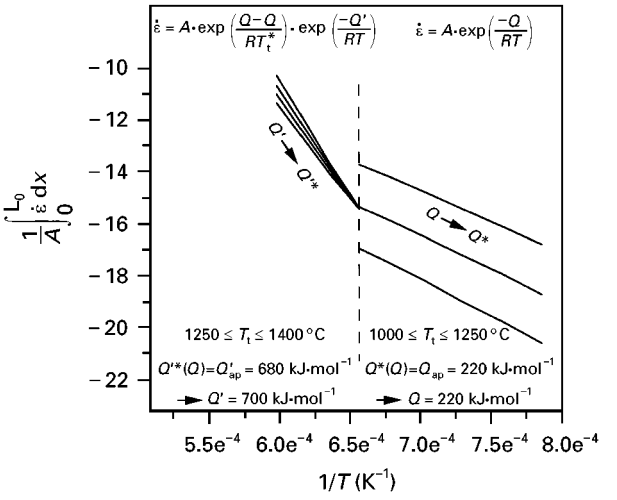

Figure 20 Temperature dependence of the calculated elongation rate as a function of the activation energy (Q).

for $1000 \leqslant T \leqslant 1250\,^{\circ}\mathrm{C}$, with $Q = 220 \pm 17\ \mathrm{kJ \cdot mol^{-1}}$, and

$$\dot{\varepsilon} = A \cdot \exp\left(\frac{Q - Q'}{RT_t^*}\right) \cdot \exp\left(\frac{-Q'}{RT}\right) \tag{A9}$$

for $1250 \leqslant T \leqslant 1400\,^{\circ}\mathrm{C}$ ($T_t^* = 1523$ K).

Apparent activation energies $Q'^*(Q')$ were derived from the calculation of ΔL_{oT_t} from Equations A4, A2 and A9, for T_t values ranging $1250 \leqslant T_t \leqslant 1400\,^{\circ}\mathrm{C}$ (Fig. 20). The activation energy of steady state creep strain rate Q' for $1250 \leqslant T \leqslant 1400\,^{\circ}\mathrm{C}$, is the solution of

$$Q'^*(Q') = Q'_{ap} \tag{A10}$$

with $Q'_{ap} = 680\ \mathrm{kJ \cdot mol^{-1}}$ i.e., $Q' = 700 \pm 30\ \mathrm{kJ \cdot mol^{-1}}$.

Q and A being determined, the equivalent gauge length L_{eT_t} (i.e., the isothermal fibre length whose elongation rate $\Delta \dot{L}_{oT_t}$ would be equal to the experimental value) and the steady state creep strains $\dot{\varepsilon}_{oT_t}$ can both be calculated. Combining Equations A1 and A4, one has:

$$L_{eT_t} = \int_0^{L_o} \frac{\exp\left(\dfrac{-Q}{RT_t \cdot g_T(x)}\right)}{\exp\left(\dfrac{-Q}{RT_t}\right)}\,dx$$

$$= \int_0^{L_o} \exp\left(\frac{-Q}{RT_t}\left(1 - \frac{1}{g_T(x)}\right)\right)dx \tag{A11}$$

and finally:

$$\dot{\varepsilon}_{oT_t} = \frac{\Delta \dot{L}_{oT_t}}{L_{eT_t}} \tag{A12}$$

Equivalent gauge length values are rather close, whatever the testing temperature, as suggested by the $g_T(x)$ profiles (Fig. 2). They are of the order of $L_{eT_t} = 62.5 \pm 2.5$ mm, for $1000 \leqslant T \leqslant 1400\,^{\circ}\mathrm{C}$.

It is noteworthy that the assessment of creep strain is rigorous for stationary creep behaviour. Nevertheless, Equation A10 has also been used to determine the primary creep strain and thus, to plot the whole creep curves (Figs 9, 13, 14).

Appendix 2. Calculation of the Young's modulus of ceramic fibres at high temperature from tensile tests with cold grips

(1) Calculation method

During the tensile test with cold grips, the temperature is not uniform along the fibre (Fig. 5). The temperature varies from ambient (at the ends) to the testing temperature T_e (in the middle). The total strain of the fibre, can be considered as the addition of elemental strains of isothermal lengths $\Delta_{Te}(T_i)$, whose temperature is $T_i = i.\delta T$ (with δT a constant) and whose Young's modulus is equal to $E(T)$.

If L_o is the gauge length and $E_a(T_e)$ the apparent Young's modulus (the stress/total elongation ratio) one has:

$$\frac{L_o}{E_a(T_e)} = \sum_{i=0}^{Te/\delta T} \frac{\Delta_{Te}(T_i)}{E(T_i)} \tag{A13}$$

with $0 \leqslant T_e \leqslant T_{e_{max}}$ and $T_i = i \cdot \delta T$

$$E(T_j) = \frac{\Delta_{(Tj)}(T_j)}{\dfrac{L_0}{E_a(T_j)} - \sum_{i=0}^{j-1} \dfrac{\Delta_{(Tj)}(T_i)}{E_a(T_i)}} \tag{A14}$$

or

with $0 \leqslant j \leqslant T_{e_{max}}/\delta T$ and $T_j = j \cdot \delta T$.

All the $E(T_j)$ values ($0 \leqslant T_j \leqslant T_{e_{max}}$) can thus be recurrently assessed according to Equation A12.

(ii) Calculation of the functions $E_a(T)$ and $\Delta_{Te}(T)$

The function $E_a(T)$ ($0 \leqslant T \leqslant T_{e_{max}}$) is inferred from the interpolation of the experimental curve $E_a = f(T_e)$ (Fig. 19).

In order to calculate the $\Delta_{Te}(T)$ values with $0 < T < T_e < T_{e_{max}}$, the temperature profile along the fibre axis is required for each testing temperature (Fig. 5). For a given δT value (here chosen equal to $100\,^{\circ}\mathrm{C}$), the distribution of the isothermal lengths $\Delta_{Te}(T)$ as a function of T_e can thus be determined. The $E(T)$ function can be easily inferred from Equation A12 (Fig. 19). The error of the $E(T)$ value, based on the experimental $E_a(T)$ deviations, has been evaluated from Equation A12 (Fig. 19).

Acknowledgements

Funding for this work and student' bursary were supplied by CNRS and SEP. The authors gratefully thank R. Bodet for his valuable advice on creep test measurements. We also thank F. Laanani, M. Monthioux of Laboratoire Marcel Mathieu, Pau, for the TEM microscopy.

References

1. J. L. CHERMANT, Presses du CNRS, (1989).
2. A. R. BUNSEL, in "Ceramics Mature Composites", edited by R. Warren (Blackie, Glasgow, 1992) p. 12.
3. M. H. LEWIS, *The Institute of Metals London* **392** (1986) 1–20.
4. N. BIRKS and F. S. PETTIT, *Mat. Sci. and Engng.* **A143** (1991) 187.
5. D. J. JOHNSON, in "Introduction to carbon science" edited by H. Marsh (Butterworths, London, 1989) p. 197.
6. M. S. DRESSELHAUS, G. DRESSELHAUS, K. SUGIHARA, I. L. SPAIN and H. A. GOLBERG, in "Graphite Fibres and Filaments" edited by M. Cardona (Springer Verlag, London, 1988) p. 230.
7. F. LAMOUROUX, X. BOURRAT, R. NASLAIN and J. SEVELY, *Carbon* **31** (1993) 1273.
8. D. J. PYSHER and R. E. TRESSLER, *J. Mater. Sci.* **27** (1992) 423.
9. D. M. WILSON, D. C. LUENBURG and S. L. LIEDER, *Ceram. Engng. Sci. Proc.* **14** (1993) 609.
10. G. N. MORSHER, K. C. CHEN and K. S. MAZDIYASNI, *ibid.* **15** (1994) 181.
11. P. J. JORGENSEN, M. E. WADSWORTH and I. B. CUTLER, *J. Amer. Ceram. Soc.* **42** (1959) 613.
12. J. A. COSTELLO and R. E. TRESSLER *ibid.* **64** (1981) 327.
13. S. YAJIMA, J. HAYASHI and M. OMORI, *Chem. Lett.* **9** (1975) 931.
14. S. YAJIMA, K. OKAMURA and J. HAYASHI, *ibid* **1** (1975) 1209.
15. C. LAFFON, A. M. FLANCK, P. LAGARDE, M. LARIDJANI, R. HAGEGE, P. OLRY, J. COTTERET, J. DIXMIER, J. L. MIQUEL, H. HAMMEL and A. P. LEGRAND, *J. Mater. Sci.* **24** (1989) 1503.

16. L. PORTE and A. SARTRE, *ibid* **24** (1989) 271.
17. P. LE COUSTUMER, M. MONTHIOUX and A. OBERLIN, J. Eur. Ceram. Soc. **11** (1993) 95.
18. T. MAH, N. LECHT, D. E. Mc CULLUM, J. R. HOENIGMAN, H. M. KIM, A. P. KATZ and H. A. LIPSITT, *J. Mater. Sci.* **19** (1984) 1191.
19. T. J. CLARK, R. M. ARONS, I. B. STAMATOFF and J. RABE, *Ceram. Engng. and Sci. Proc.* **6** (1985) 576.
20. S. M. JOHNSON, R. D. BRITTAIN, R. H. LAMOREAU and D. J. ROWCLIFFE, *J. Amer. Ceram. Soc.* **71** (1988) C-132.
21. T. SHIMOO, H. CHEN and K. OKAMURA, *J. Ceram. Soc. Jpn* **100** (1991) 48.
22. M. H. JASKOWIAK and J. A. DI CARLO, *J. Amer. Ceram. Soc.* **72** (1989) 192.
23. B. A. BENDER, J. S. WALLACE and D. J. SCHRODT, *J. Mater Sci.* **26** (1991) 970.
24. N. JIA, R. BODET and R. E. TRESSLER, *J. Amer. Ceram. Soc.* **76** (1993) 3051.
25. R. BODET, J. LAMON, N. JIA and R. E. TRESSLER, *ibid.* (in press).
26. K. OKAMURA, M. SATO, T. SEGUSHI and S. KAWANISHI, in "Controlled Interphases in Composite Materials" edited by H. Ishida (Elsevier, New York 1990) p. 209.
27. M. TAKEDA, Y. IMAI, H. ICHIKAWA, T. ICHIKAWA, N. KASAI, T. SEGUSHI and K. OKAMURA, *Ceram. Engng. Sci. Proc.* **13** (1992) 209.
28. *Idem*, *ibid.* **14** (1993) 540.
29. R. BODET, X. BOURRAT, J. LAMON and R. NASLAIN, *J. Mater. Sci.* **30** (1995) 661.
30. G. CHOLLON, C. LAPORTE, R. PAILLER, R. NASLAIN, F. LAANANI, M. MONTHIOUX and P. OLRY, *ibid.* **32** (1997) 327.
31. G. N. MORSHER and J. A. DI CARLO, *J. Amer. Ceram. Soc.* **75** (1992) 136.
32. J. A. DI CARLO, *Comp. Sci. and Techn.* **51** (1994) 213.
33. J. F. VILLENEUVE, D. MOCAER, R. PAILLER, R. NASLAIN and P. OLRY, *J. Mater. Sci.* **28** (1993) 1227.
34. P. ROCABOIS, thesis, Institut National Polytechnique de Grenoble, (1993).
35. D. J. PYSHER, K. C. GORETTA, R. S. HODDER Jr and R. E. TRESSLER, *J. Amer. Ceram. Soc.* **72** (1989) 284.
36. J. W. BEALE, E. LARA-CURZIO and S. S. STERNSTEIN, Int. Sampl. Symp. Exhib. (1990) 35 (2, Adv. Mater.: Challenge Next Decade) p. 1193–204.
37. R. BACON and W. H. SMITH, In Proc 2nd Conference on Industrial Carbon and Graphite, London edited by the Soc. Chem. Ind. (Gordon and Breach, New York, 1965) p. 203.
38. M. H. HON and R. F. DAVIS, *J. Mater. Sci.* **14** (1979) 2411.
39. M. H. HON, R. F. DAVIS and D. E. NEWBURRY, *Ibid.* **15** (1980) 2073.
40. L. GREEN Jr, in Proceedings of the Fourth Conf. on Carbon, Buffalo, 1959 (Pergamon, NY, 1960) p. 497.
41. H. W. DAVIDSON and H. H. W. LOSTY, *ibid.* p. 585.
42. J. F. ANDREW and S. SATO, *Carbon* **1** (1964) 225.
43. J. G. MORLEY, High Performance Fibre Composite (Academic Press, 1987) 21.

Received 19 April
and accepted 21 May 1996